Greenland temperature response to climate forcing during the last deglaciation

Christo Buizert *et al.*

Science **345**, 1177 (2014);
DOI: 10.1126/science.1254961

7. S. M. Sowell *et al.*, *ISME J.* **3**, 93–105 (2009).
8. R. M. Morris *et al.*, *ISME J.* **4**, 673–685 (2010).
9. Materials and Methods are available on *Science* online.
10. G. Reygondeau *et al.*, *Global Biogeochem. Cycles* **27**, 1046–1058 (2013).
11. R. M. Gordon, K. H. Coale, K. S. Johnson, *Limnol. Oceanogr.* **42**, 419–431 (1997).
12. D. M. Karl, R. R. Bidigare, R. M. Letelier, *Deep Sea Res. Part II Top. Stud. Oceanogr.* **48**, 1449–1470 (2001).
13. F. Partensky, W. R. Hess, D. Vaulot, *Microbiol. Mol. Biol. Rev.* **63**, 106–127 (1999).
14. V. Lange *et al.*, *Mol. Cell. Proteomics* **7**, 1489–1500 7(2008).
15. J. LaRoche, P. W. Boyd, R. M. L. McKay, R. J. Geider, *Nature* **382**, 802–805 (1996).
16. A. W. Thompson, K. Huang, M. A. Saito, S. W. Chisholm, *ISME J.* **5**, 1580–1594 (2011).
17. D. Lindell, E. Padan, A. F. Post, *J. Bacteriol.* **180**, 1878–1886 (1998).
18. A. C. Tolonen *et al.*, *Mol. Syst. Biol.* **2**, 53 (2006).
19. G. Rocap, D. L. Distel, J. B. Waterbury, S. W. Chisholm, *Appl. Environ. Microbiol.* **68**, 1180–1191 (2002).
20. L. O. Slemons, J. W. Murray, J. Resing, B. Paul, P. Dutrieux, *Global Biogeochem. Cycles* **24**, GB3024 (2010).
21. L. R. Moore, A. F. Post, G. Rocap, S. W. Chisholm, *Limnol. Oceanogr.* **47**, 989–996 (2002).
22. J. R. Casey, M. W. Lomas, J. Mandecki, D. E. Walker, *Geophys. Res. Lett.* **34**, L10604 (2007).
23. B. Wawrik, A. V. Callaghan, D. A. Bronk, *Appl. Environ. Microbiol.* **75**, 6662–6670 (2009).
24. N. A. Kamennaya, A. F. Post, *Limnol. Oceanogr.* **58**, 1959–1971 (2013).
25. A. C. Martiny, S. Kathuria, P. M. Berube, *Proc. Natl. Acad. Sci. U.S.A.* **106**, 10787–10792 (2009).
26. G. R. DiTullio, D. A. Hutchins, K. W. Bruland, *Limnol. Oceanogr.* **38**, 495–508 (1993).
27. D. B. Rusch, A. C. Martiny, C. L. Dupont, A. L. Halpern, J. C. Venter, *Proc. Natl. Acad. Sci. U.S.A.* **107**, 16184–16189 (2010).
28. M. A. Saito, J. W. Moffett, S. W. Chisholm, J. B. Waterbury, *Limnol. Oceanogr.* **47**, 1629–1636 (2002).
29. A. C. Martiny, M. L. Coleman, S. W. Chisholm, *Proc. Natl. Acad. Sci. U.S.A.* **103**, 12552–12557 (2006).
30. B. A. S. Van Mooy, G. Rocap, H. F. Fredricks, C. T. Evans, A. H. Devol, *Proc. Natl. Acad. Sci. U.S.A.* **103**, 8607–8612 (2006).
31. S. M. Birkey, W. Liu, X. Zhang, M. F. Duggan, F. M. Hulett, *Mol. Microbiol.* **30**, 943–953 (1998).
32. I. Mary, D. Vaulot, *FEMS Microbiol. Lett.* **226**, 135–144 (2003).
33. A. E. Noble, M. A. Saito, K. Maiti, C. Benitez-Nelson, *Deep Sea Res. Part II Top. Stud. Oceanogr.* **55**, 1473–1490 (2008).
34. J. J. Polovina, J. P. Dunne, P. A. Woodworth, E. A. Howell, *ICES J. Mar. Sci.* **68**, 986–995 (2011).
35. P. W. Boyd, R. Strzepek, F. Fu, D. A. Hutchins, *Limnol. Oceanogr.* **55**, 1353–1376 (2010).
36. P. Flombaum *et al.*, *Proc. Natl. Acad. Sci. U.S.A.* **110**, 9824–9829 (2013).

ACKNOWLEDGMENTS

This work was made possible by NSF grants OCE-1031271, 1155566, and 1233261 Gordon Betty Moore Foundation grants 2724 and 3782, the Center for Microbial Research and Education, and the Woods Hole Oceanographic Institution Ocean Life Institute. We are grateful to the captain and crew of the R/V *Kilo Moana*, particularly V. Polidoro for his resourcefulness. We thank N. Hawco, D. Wang, and P. Balcom for sampling assistance and J. Dusenberry for programming assistance. We thank A. Santoro, J. Waterbury, and P. Chivers for helpful discussions and J. Blethrow and V. Zabrouskov (Thermo Scientific) for analyses on the prototype Fusion. Data for the Metyme Expedition are available at www.bco-dmo.org.

SUPPLEMENTARY MATERIALS

www.sciencemag.org/content/345/6201/1173/suppl/DC1
Materials and Methods
Supplementary Text
Figs. S1 to S18
Tables S1 to S6
References (*37*–*63*)

23 May 2014; accepted 25 July 2014
10.1126/science.1256450

PALEOCLIMATE

Greenland temperature response to climate forcing during the last deglaciation

Christo Buizert,[1]* Vasileios Gkinis,[2,3] Jeffrey P. Severinghaus,[4] Feng He,[5] Benoit S. Lecavalier,[6] Philippe Kindler,[7] Markus Leuenberger,[7] Anders E. Carlson,[1] Bo Vinther,[2] Valérie Masson-Delmotte,[8] James W. C. White,[3] Zhengyu Liu,[5,9] Bette Otto-Bliesner,[10] Edward J. Brook[1]

Greenland ice core water isotopic composition ($\delta^{18}O$) provides detailed evidence for abrupt climate changes but is by itself insufficient for quantitative reconstruction of past temperatures and their spatial patterns. We investigate Greenland temperature evolution during the last deglaciation using independent reconstructions from three ice cores and simulations with a coupled ocean-atmosphere climate model. Contrary to the traditional $\delta^{18}O$ interpretation, the Younger Dryas period was 4.5° ± 2°C warmer than the Oldest Dryas, due to increased carbon dioxide forcing and summer insolation. The magnitude of abrupt temperature changes is larger in central Greenland (9° to 14°C) than in the northwest (5° to 9°C), fingerprinting a North Atlantic origin. Simulated changes in temperature seasonality closely track changes in the Atlantic overturning strength and support the hypothesis that abrupt climate change is mostly a winter phenomenon.

The last deglaciation [~19 thousand to 11 thousand years before the present (ky B.P.)] is the most recent example of natural global warming and large-scale climate reorganization, providing an exceptional opportunity to study the interaction between different components of the climate system (*1*) and climate sensitivity to changes in radiative forcing (*2*). Much of the regional and global climate variability of this period can be explained as the superposition of two distinct modes (*3*, *4*): a global increase in surface temperature related to increased radiative forcing (Fig. 1C) and an interhemispheric redistribution of heat associated with variability in the Atlantic meridional overturning circulation (AMOC) strength (Fig. 1D).

High-resolution records of Northern Hemisphere (NH) high-latitude climate are provided by Greenland ice core water isotopic composition ($\delta^{18}O$ and δD), a proxy for local condensation temperature (Fig. 1A). Past water isotopic variations reflect site temperature (T_{site}) to first order (*5*) but are also influenced by changes to the atmospheric hydrological cycle, such as evaporation conditions (*6*, *7*), moisture origin and transport pathways (*8*, *9*), and precipitation intermittency or seasonality (*10*). Assuming a linear $\delta^{18}O$-T_{site} relationship suggests that Greenland climate did not begin to warm until the Bølling onset (14.7 ky B.P.), lagging much of the globe and implying a negligible Greenland temperature response to increasing atmospheric CO_2 (*11*–*14*). Such delayed Arctic warming is hard to reconcile with past sea levels and NH ice sheet extent that indicate substantial ice loss before the Bølling (*15*). This paradox is exemplified by lower Greenland summit $\delta^{18}O$ levels during the Younger Dryas period (YD, 12.8 to 11.7 ky B.P.) than during the Oldest Dryas period (OD, 18 to 14.7 ky B.P.), despite the rise in boreal summer insolation (Fig. 1B) and a ~50 parts per million increase in atmospheric CO_2 (*14*, *16*).

Accurate temperature reconstructions are required to improve our understanding of the mechanisms controlling Greenland climate during the last deglaciation and to benchmark transient climate simulations (*17*, *18*). Here, we circumvent the issues that confound water isotope interpretation by using four independent temperature reconstructions from three ice cores

[1]College of Earth, Ocean, and Atmospheric Sciences, Oregon State University, Corvallis, OR 97331, USA. [2]Centre for Ice and Climate, Niels Bohr Institute, University of Copenhagen, Denmark. [3]Institute of Arctic and Alpine Research, University of Colorado, Boulder, CO 80309, USA. [4]Scripps Institution of Oceanography, University of California–San Diego, La Jolla, CA 92093, USA. [5]Center for Climatic Research, Nelson Institute for Environmental Studies, University of Wisconsin, Madison, WI 53706, USA. [6]Department of Physics and Physical Oceanography, Memorial University, St. John's, Canada. [7]Division of Climate and Environmental Physics, Physics Institute and Oeschger Centre for Climate Change Research, University of Bern, Bern, Switzerland. [8]Laboratoire des Sciences du Climat et de l'Environnement, Institut Pierre Simon Laplace (UMR CEA-CNRS-UVSQ 8212), Gif-sur-Yvette, France. [9]Laboratory for Climate and Ocean-Atmosphere Studies, Peking University, Beijing 100871, China. [10]Climate and Global Dynamics Division, National Center for Atmospheric Research, Boulder, CO 80307, USA.
***Corresponding author. E-mail: buizertc@science.oregonstate.edu**

[North Greenland Eemian Ice Drilling (NEEM), North Greenland Ice Core Project (NGRIP), and Greenland Ice Sheet Project 2 (GISP2)] (Fig. 1, G to I), which we combine with transient general circulation model (GCM) simulations (*4*, *16*, *17*). Our work provides a consistent picture of the temporal, spatial, and seasonal trends in the Greenland surface temperature response to external (insolation) and internal (CO_2, AMOC, and ice topography) climate forcings during the last deglaciation.

Our primary T_{site} reconstruction method uses gas-phase $\delta^{15}N$-N_2 data (Fig. 1F) and the inversion of a dynamical firn densification model to find the T_{site} history that optimizes the fit to the $\delta^{15}N$ data through an automated algorithm. The method builds on earlier $\delta^{15}N$ work, in which mostly the abrupt transitions were investigated (*5*, *19*–*21*). Our approach also allows investigation of T_{site} evolution between abrupt transitions and robustly quantifies the uncertainty associated with the temperature reconstruction by exploring 216 combinations of densification physics and model parameters at each site. Details on the method are given in figs. S1 to S7 (*22*). For the NGRIP core, a second reconstruction method uses the temperature sensitivity of water isotope diffusion in the firn column (*23*). The isotope diffusion length is calculated along the core from high-resolution $\delta^{18}O$ data using spectral techniques. T_{site} is estimated from the diffusion length after accounting for firn densification, solid ice diffusion, and thinning due to ice flow. We perform a sensitivity study with 2000 reconstructions in which values of four key diffusion model parameters are altered. Both NGRIP reconstructions agree within uncertainty, and we therefore average the results. We further use transient climate simulations performed with the coupled ocean-atmosphere Community Climate System Model version 3 (CCSM3), which have been shown to capture correctly many aspects of deglacial climate history (*4*, *11*, *16*, *17*). The CCSM3 model has an equilibrium climate sensitivity of 2.3°C for a doubling of CO_2 (T31 grid), which is within the range of estimates from the Intergovernmental Panel on Climate Change (*24*).

First, we investigate the temperature difference between the YD and OD periods. Our reconstruction methods yield an ensemble of T_{site} reconstructions for each site, and we bin the results (Fig. 2A). For comparison, mean annual surface air temperature (SAT) changes from the GCM simulations are marked in black on the horizontal axes. All four reconstructions show that the YD period was warmer than the OD, on average by 4.5° ± 2°C (1 SD uncertainty). This contrasts with summit $\delta^{18}O$, which is more strongly depleted during the YD than the OD (*12*, *13*). Our reconstruction is consistent with increased CO_2 and boreal summer insolation during the YD relative to the OD (*16*), as well as NH non–ice core proxy synthesis results (Fig. 1E) that also exhibit a positive YD-OD difference (*11*). CCSM3 reproduces our reconstructed YD-OD warming well, simulating a 5.4°C YD-OD difference averaged over the sites. Transient simulations with an Earth system model of intermediate complexity also find a ~5°C YD-OD temperature difference (*18*). Our reconstructions are thus compatible with current understanding of the role of CO_2 forcing on climate. Additional CCSM3 simulations in which the different climatic forcings are isolated (*4*) suggest that the YD-OD warming due to greenhouse gas forcing is about three times as large as the warming caused by increased insolation (fig. S9). The T_{site} reconstructions show a poleward enhancement of the YD-OD signal, with warming being largest at the NEEM site. This spatial pattern is also captured in the CCSM3 model response (Fig. 2E). Whereas homogeneous Greenland warming is simulated in response to increased CO_2 or insolation, changes in the Laurentide ice sheet topography induce atmospheric circulation changes that affect North Atlantic climate and can explain the observed spatial gradient (fig. S9).

Second, we investigate the abrupt climatic events that are superimposed on the gradual warming of the background climate; the magnitudes of the abrupt warming/cooling (ΔT) at the Bølling (14.7 ky B.P.), YD (12.8 ky B.P.), and Holocene (11.6 ky B.P.) onset are shown in Fig. 2,

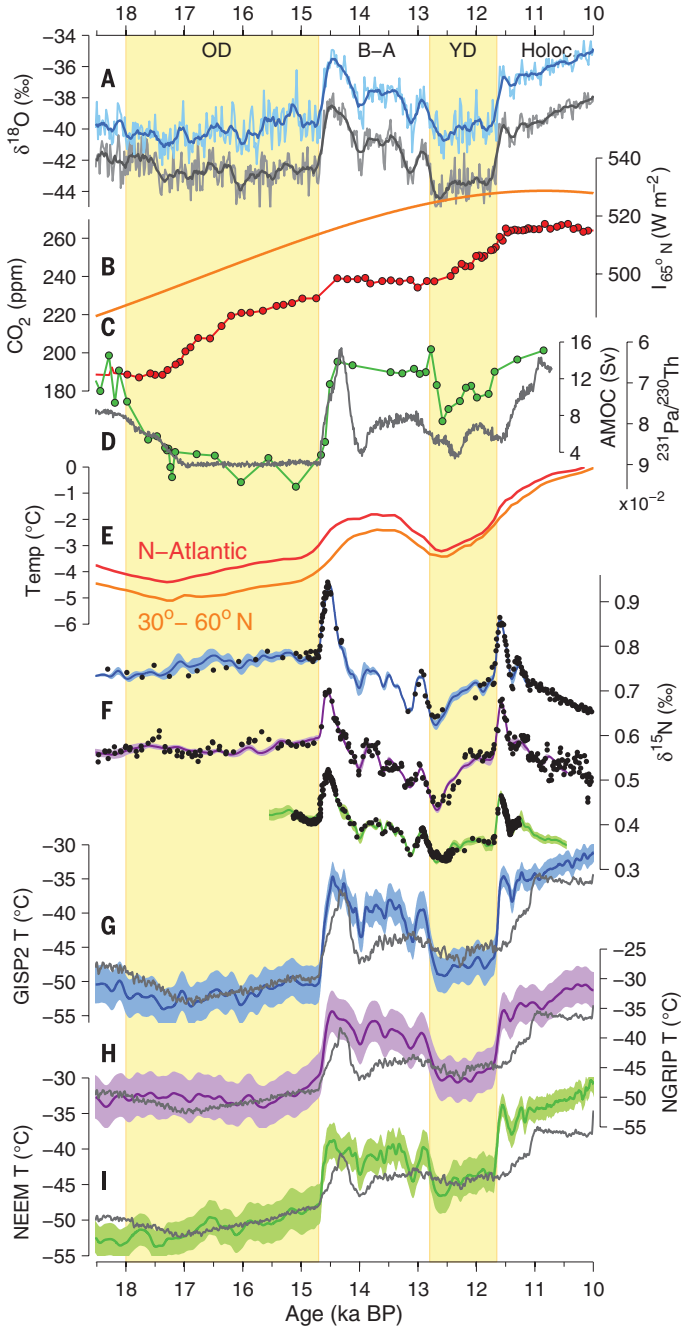

Fig. 1. Paleoclimate records and Greenland temperature reconstructions for the last deglaciation. (**A**) Greenland summit ice core $\delta^{18}O$ from GISP2 (blue) and GRIP [gray, offset by −3 per mil (‰) for clarity]. (**B**) The 21 June insolation at 65°N. (**C**) Atmospheric CO_2 mixing ratios (*14*). (**D**) Bermuda rise (core OCE326-GGC5) $^{231}Pa/^{230}Th$ as a proxy for AMOC strength (green) (*30*) and GCM AMOC strength (gray) in sverdrups (1 Sv = 10^6 m^3 s^{-1}). (**E**) Surface temperature stacks for 30°N to 60°N and North Atlantic region (*11*). (**F**) GISP2 (blue, offset by +0.3‰ for clarity), NGRIP (purple, +0.15‰ offset) and NEEM (green) model fit to $\delta^{15}N$ data (black dots). (**G** to **I**) Greenland temperature reconstructions with ±1 SD uncertainty envelope for GISP2 (blue), NGRIP (purple), NEEM (green), and CCSM3 GCM output (gray) (*16*, *17*).

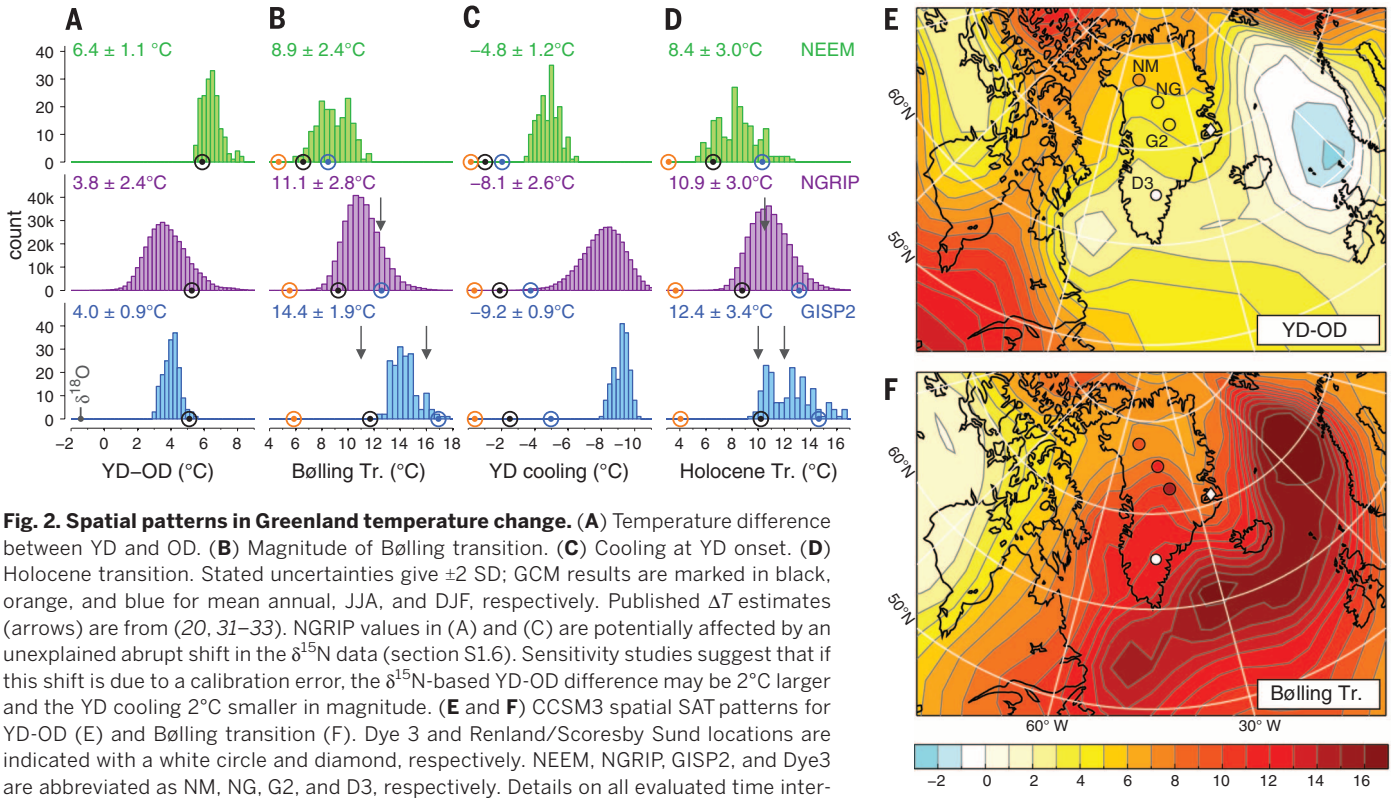

Fig. 2. Spatial patterns in Greenland temperature change. (**A**) Temperature difference between YD and OD. (**B**) Magnitude of Bølling transition. (**C**) Cooling at YD onset. (**D**) Holocene transition. Stated uncertainties give ±2 SD; GCM results are marked in black, orange, and blue for mean annual, JJA, and DJF, respectively. Published ΔT estimates (arrows) are from (*20*, *31*–*33*). NGRIP values in (A) and (C) are potentially affected by an unexplained abrupt shift in the $\delta^{15}N$ data (section S1.6). Sensitivity studies suggest that if this shift is due to a calibration error, the $\delta^{15}N$-based YD-OD difference may be 2°C larger and the YD cooling 2°C smaller in magnitude. (**E** and **F**) CCSM3 spatial SAT patterns for YD-OD (E) and Bølling transition (F). Dye 3 and Renland/Scoresby Sund locations are indicated with a white circle and diamond, respectively. NEEM, NGRIP, GISP2, and Dye3 are abbreviated as NM, NG, G2, and D3, respectively. Details on all evaluated time intervals are given in table S1 (*22*).

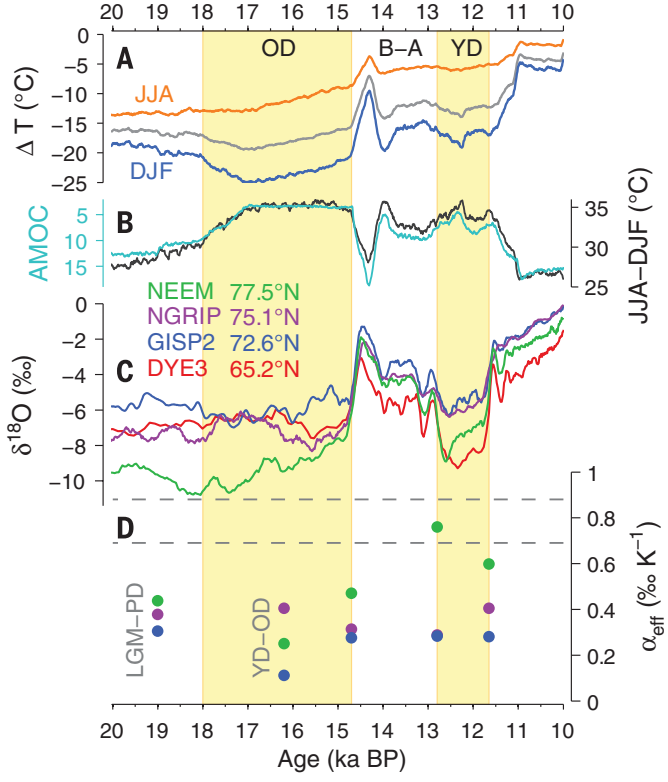

Fig. 3. Greenland isotopes and temperature seasonality. (**A**) Simulated summer (JJA), winter (DJF), and mean annual temperatures (gray) relative to the present day at Scoresby Sund (Fig. 2F), the site studied by Denton *et al*. (*26*). (**B**) CCSM3 temperature seasonality JJA-DJF (gray) and AMOC strength in sverdrups (turquoise). (**C**) $\delta^{18}O$ of four Greenland ice cores corrected for mean oceanic $\delta^{18}O$, relative to present-day $\delta^{18}O$. (**D**) Effective isotopic temperature sensitivity for GIPS2 (blue dots), NGRIP (purple), and NEEM (green), with present-day spatial isotope sensitivity (0.69 ‰ K^{-1}) and Rayleigh-type distillation model prediction (0.88 ‰ K^{-1}) (dashed lines).

B to D. At all sites, ΔT is larger at the Bølling transition than at the Holocene transition. For all three abrupt events, ΔT is smallest (5° to 9°C) in northwest Greenland (NEEM) and largest (9° to 14°C) in central Greenland (GISP2). This spatial gradient, which is not reflected in $\delta^{18}O$, is also observed for several Dansgaard-Oeschger events (*19*), suggesting that it is a robust feature of abrupt climate change over Greenland. CCSM3 fails to reproduce the timing of the Holocene transition and underestimates the ΔT magnitude of the Bølling and Holocene transitions by ~20% and the magnitude of the YD cooling by ~75%. Yet CCSM3 qualitatively captures the observed spatial ΔT gradient. In the simulations, AMOC invigoration at the Bølling onset is associated with maximum SAT change in the North Atlantic (Fig. 2F) due to increased northward oceanic heat transport and an associated reduction in sea-ice cover (fig. S10). As a result, the simulated SAT changes are largest for ice core sites closest to the North Atlantic (i.e., GISP2) and smallest in northwest Greenland.

In the simulations, AMOC variations are induced by a freshwater forcing to the North Atlantic, using a meltwater discharge scenario designed to be broadly consistent with available evidence of past sea level, ice sheet extent, and meltwater routing (*15*). We recognize that processes other than freshwater may have contributed to, and perhaps even caused, the AMOC and sea-ice variations of the deglaciation. Regardless of its cause, AMOC invigoration will

result in North Atlantic warming and a reduction in sea-ice cover, which in turn affects the atmospheric circulation and Greenland SAT. Atmosphere-only GCM experiments of North Atlantic sea-ice removal under Last Glacial Maximum (LGM) conditions show a ΔT pattern qualitatively similar to that simulated by CCSM3, suggesting that sea-ice variability by itself may be sufficient to explain this pattern (*25*). The northward reduction in ΔT magnitude that we reconstruct over Greenland is thus likely a fingerprint of the North Atlantic origin of abrupt climate change, irrespective of the precise roles played by freshwater forcing and AMOC variations.

Our T_{site} reconstructions provide annual mean temperatures, and to investigate seasonal temperature changes we turn to the CCSM3 simulations. Simulated Greenland temperature seasonality is strongly linked to AMOC strength and mean climate state, with large (small) seasonality during periods of weak (strong) overturning (Fig. 3B). Most of the seasonality signal is due to winter [December to February (DJF)] SAT, which changes more than summer [June to August (JJA)] SAT (Fig. 3A). The dominance of winter SAT is most clearly manifested during abrupt transitions, where simulated DJF ΔT (marked blue in Fig. 2, B to D) is much larger than JJA ΔT (orange). This contrasts with the (primarily CO_2-forced) YD-OD warming, for which DJF and JJA warming are nearly identical (within 10% of the mean annual change). Our simulations thus support the hypothesis that abrupt climate change is mostly a winter phenomenon (*25*–*28*). In the simulations, reduced AMOC strength and attendant heat transport (such as during the YD and OD) results in an extensive North Atlantic winter sea-ice cover (fig. S10). This extended sea ice, in turn, insulates the atmosphere from the moderating influence of the large oceanic heat capacity, resulting in extremely low winter SAT and increased temperature seasonality over Greenland. Because ablation of land-based ice occurs primarily during summer months, summer SAT is the main control on continental ice volume (*26*). If AMOC variability mainly affects winter SAT, as suggested by the CCSM3 simulations, it has only a limited effect on margin positions and ice volume, which may in part explain the paucity of YD moraines found across Greenland (*29*) and the continued sea-level rise across the OD and YD intervals (*15*). Our temperature reconstructions, as well as the strong AMOC-seasonality link we simulate, can inform efforts to understand and model Greenland ice sheet evolution during the deglaciation.

The independent reconstructions can be used to investigate nontemperature influences on $\delta^{18}O$. To this end, we calculate the effective isotope sensitivity $\alpha_{eff} = \Delta\delta^{18}O_{corr}/\Delta T$, with $\Delta\delta^{18}O_{corr}$ the change in $\delta^{18}O$ (corrected for mean ocean $\delta^{18}O$) associated with temperature change ΔT (Fig. 3D). As in other studies (*5*, *19*, *20*), we find that α_{eff} varies both between sites and in time, showing the limitations of the $\delta^{18}O$ paleothermometer. On average, α_{eff} at NEEM is closest to sensitivity values obtained from the present-day spatial $\delta^{18}O$-T_{site} relationship and Rayleigh-type distillation models (*7*). Going southward, α_{eff} decreases, reflecting an increasing net effect of nontemperature influences on $\delta^{18}O$. This meridional gradient in $\delta^{18}O$ bias is further demonstrated by the Dye3 core in south Greenland (Fig. 3C), where the YD-OD $\delta^{18}O$ anomaly is most pronounced. GCM simulations suggest that changes in precipitation seasonality most strongly affect South Greenland, in general agreement with the meridional α_{eff} gradient that we observe (fig. S11B). Moisture tracking in the CCM3 atmospheric GCM (*8*), furthermore, suggests an increased relative contribution of (strongly distilled) Pacific vapor during the LGM, which is most pronounced at NEEM (fig. S11A) and consistent with the observed stronger glacial $\delta^{18}O$ depletion at NEEM. The apparently stable and high α_{eff} values at NEEM may be caused by compensating $\delta^{18}O$ biases and do not necessarily imply a more faithful $\delta^{18}O$ paleothermometer. Our T_{site} reconstructions can be used in conjunction with GCM isotope modeling to unravel the ice core water isotopic signals ($\delta^{18}O$, deuterium excess, and ^{17}O excess), potentially providing constraints on atmospheric circulation changes during the last deglaciation.

In summary, our independent temperature reconstructions reveal the magnitude and spatial structure of deglacial Greenland temperature changes, for which $\delta^{18}O$ by itself does not provide reliable, quantitative information. Our work demonstrates the role of CO_2 in forcing Greenland climate during the last deglaciation, shows a spatial pattern of the abrupt deglacial transitions that fingerprints a North Atlantic origin, and identifies an important connection between AMOC strength and temperature seasonality. These results provide a valuable target to benchmark transient climate model simulations, can help refine estimates of past climate sensitivity, and can provide realistic climate forcing for Greenland ice sheet models during the last deglaciation.

REFERENCES AND NOTES

1. P. U. Clark *et al.*, *Proc. Natl. Acad. Sci. U.S.A.* **109**, E1134–E1142 (2012).
2. E. J. Rohling *et al.*, *Nature* **491**, 683–691 (2012).
3. J. D. Shakun, A. E. Carlson, *Quat. Sci. Rev.* **29**, 1801–1816 (2010).
4. F. He *et al.*, *Nature* **494**, 81–85 (2013).
5. C. Huber *et al.*, *Earth Planet. Sci. Lett.* **243**, 504–519 (2006).
6. E. A. Boyle, *Geophys. Res. Lett.* **24**, 273–276 (1997).
7. V. Masson-Delmotte *et al.*, *Science* **309**, 118–121 (2005).
8. P. L. Langen, B. M. Vinther, *Clim. Dyn.* **32**, 1035–1054 (2009).
9. C. D. Charles, D. Rind, J. Jouzel, R. D. Koster, R. G. Fairbanks, *Science* **263**, 508–511 (1994).
10. M. Werner, U. Mikolajewicz, M. Heimann, G. Hoffmann, *Geophys. Res. Lett.* **27**, 723–726 (2000).
11. J. D. Shakun *et al.*, *Nature* **484**, 49–54 (2012).
12. K. M. Cuffey, G. D. Clow, *J. Geophys. Res.* **102** (C12), 26383 (1997).
13. R. B. Alley, *Quat. Sci. Rev.* **19**, 213–226 (2000).
14. E. Monnin *et al.*, *Science* **291**, 112–114 (2001).
15. A. E. Carlson, P. U. Clark, *Rev. Geophys.* **50**, RG4007 (2012).
16. Z. Liu *et al.*, *Proc. Natl. Acad. Sci. U.S.A.* **109**, 11101–11104 (2012).
17. Z. Liu *et al.*, *Science* **325**, 310–314 (2009).
18. L. Menviel, A. Timmermann, O. E. Timm, A. Mouchet, *Quat. Sci. Rev.* **30**, 1155–1172 (2011).
19. M. Guillevic *et al.*, *Clim. Past* **9**, 1029–1051 (2013).
20. P. Kindler *et al.*, *Clim. Past* **10**, 887–902 (2014).
21. J. P. Severinghaus, E. J. Brook, *Science* **286**, 930–934 (1999).
22. Materials and methods are available as supplementary materials on *Science* Online.
23. V. Gkinis, S. B. Simonsen, S. L. Buchardt, J. W. C. White, B. M. Vinther, *Earth Planet. Sci. Lett.* (2014); http://arxiv.org/abs/1404.4201
24. J. T. Kiehl, C. A. Shields, J. J. Hack, W. D. Collins, *J. Clim.* **19**, 2584–2596 (2006).
25. C. Li, D. S. Battisti, D. P. Schrag, E. Tziperman, *Geophys. Res. Lett.* **32**, L19702 (2005).
26. G. H. Denton, R. B. Alley, G. C. Comer, W. S. Broecker, *Quat. Sci. Rev.* **24**, 1159–1182 (2005).
27. W. S. Broecker, *Global Planet. Change* **54**, 211–215 (2006).
28. J. Flückiger, R. Knutti, J. W. C. White, H. Renssen, *Clim. Dyn.* **31**, 633–645 (2008).
29. S. Funder, K. H. Kjaer, K. K. Kjeldsen, C. Ó. Cofaigh, in *Developments in Quaternary Science, Vol. 15,* In J. Ehlers, P. L. Gibbard, P. D. Hughes, Eds. (Elsevier B.V., Amsterdam, The Netherlands, 2011).
30. J. F. McManus, R. Francois, J. M. Gherardi, L. D. Keigwin, S. Brown-Leger, *Nature* **428**, 834–837 (2004).
31. C. Goujon, J. M. Barnola, C. Ritz, *J. Geophys. Res.* **108**, 4792 (2003).
32. J. P. Severinghaus, A. Grachev, B. Luz, N. Caillon, *Geochim. Cosmochim. Acta* **67**, 325–343 (2003).
33. A. M. Grachev, J. P. Severinghaus, *Quat. Sci. Rev.* **24**, 513–519 (2005).

ACKNOWLEDGMENTS

We are are indebted in countless ways to our mentor, friend, and colleague Sigfús J. Johnsen (1940–2013). We thank S. Marcott, D. Noone, J. Rosen, P. Langen, I. Seierstad, A. Landais, B. Minster, S. Falourd, and J. Shakun for fruitful discussions or assistance. Constructive comments by two anonymous reviewers helped improve the manuscript. We acknowledge funding through NSF grants 08-06377 (J.P.S.) and 0806414 (E.J.B.), the National Oceanic and Atmospheric Administration Climate and Global Change fellowship program, administered by the University Corporation for Atmospheric Research (C.B.), Agence Nationale de la Recherche through grants ANR VMC NEEM and ANR CEPS GREENLAND (V.M.-D.), and the U.S. NSF P2C2 program (A.E.C., Z.L., F.H., and B. O.-B.). This research used resources of the Oak Ridge Leadership Computing Facility, located in the National Center for Computational Sciences at Oak Ridge National Laboratory, which is supported by the Office of Science of the Department of Energy under contract DE-AC05-00OR22725. NEEM is directed and organized by the Center of Ice and Climate at the Niels Bohr Institute and U.S. NSF, Office of Polar Programs. It is supported by funding agencies and institutions in Belgium (FNRS-CFB and FWO), Canada (NRCan/GSC), China (CAS), Denmark (FIST), France (IPEV, CNRS/INSU, CEA, and ANR), Germany (AWI), Iceland (RannIs), Japan (NIPR), Korea (KOPRI), The Netherlands (NWO/ALW), Sweden (VR), Switzerland (SNF), United Kingdom (NERC) and the USA (U.S. NSF, Office of Polar Programs). NEEM data and temperature reconstructions are provided as supplementary data files.

SUPPLEMENTARY MATERIALS

www.sciencemag.org/content/345/6201/1177/suppl/DC1
Materials and Methods
Supplementary Text
Figs. S1 to S11
Tables S1 to S3
References (*34*–*102*)

17 April 2014; accepted 31 July 2014
10.1126/science.1254961